Tunability, dielectric, and piezoelectric properties of Ba(1–x)CaxTi(1–y)ZryO3 ferroelectric thin films

Christophe Daumont, Quentin Simon, Erwan Le Mouellic, Sandrine Payan, Pascal Gardes, Patrick Poveda, Béatrice Negulescu, Mario Maglione, Jérôme Wolfman

AIP Journal of Applied Physics

Tunability, dielectric, and piezoelectric properties of Ba(1−x)CaxTi(1−y)ZryO3 ferroelectric thin films

C. J. M. Daumont, Q. Simon, E. Le Mouellic, S. Payan, P. Gardes, P. Poveda, B. Negulescu, M. Maglione, and J. Wolfman

Citation: Journal of Applied Physics **119**, 094107 (2016); doi: 10.1063/1.4942924
View online: http://dx.doi.org/10.1063/1.4942924
View Table of Contents: http://scitation.aip.org/content/aip/journal/jap/119/9?ver=pdfcov
Published by the AIP Publishing

Tunability, dielectric, and piezoelectric properties of $Ba_{(1-x)}Ca_xTi_{(1-y)}Zr_yO_3$ ferroelectric thin films

C. J. M. Daumont,[1,a)] Q. Simon,[2] E. Le Mouellic,[1] S. Payan,[2] P. Gardes,[3] P. Poveda,[3] B. Negulescu,[1] M. Maglione,[2] and J. Wolfman[1,b)]
[1]*Laboratoire GREMAN, UMR7347 CNRS, Faculté de Sciences et Techniques, Université François Rabelais, 37200 Tours, France*
[2]*Institute of Condensed Matter Chemistry of Bordeaux, ICMCB-CNRS, Université de Bordeaux, 33608 Pessac Cedex, France*
[3]*STMicroelectronics, 10 rue Thalès de Milet, 37071 Tours Cedex, France*

(Received 18 November 2015; accepted 15 February 2016; published online 3 March 2016)

Tunable ferroelectric capacitors, which exhibit a decrease of the dielectric permittivity (ϵ) under electric field, are widely used in electronics for RF tunable applications (e.g., antenna impedance matching). Current devices use barium strontium titanate as the tunable dielectric, and the need for performance enhancement of the tunable element is the key for device improvement. We report here on libraries of $Ba_{0.97}Ca_{0.03}Ti_{1-x}Zr_xO_3$ thin films ($0 \leq x \leq 27\%$) with a thickness of about 130 nm deposited on $IrO_2/SiO_2/Si$ substrates using combinatorial pulsed laser deposition allowing for gradients of composition on one sample. A total of 600 capacitors on a single sample were characterized in order to statistically investigate the dielectric properties. We show that the tunabilty is maximum at intermediate compositions, reaching values up to 60% for an electric field of about 400 kV cm^{-1}. We attribute the high tunability in the intermediate compositions to the paraelectric-ferroelectric phase transition, which is brought down to room temperature by the addition of Zr. In addition, the piezoelectric coefficient is found to be decreasing with increasing Zr content. © *2016 AIP Publishing LLC*. [http://dx.doi.org/10.1063/1.4942924]

I. INTRODUCTION

$BaTiO_3$ based ferroelectric materials have been widely used in many electronics components, such as tunable capacitors, multilayer capacitors (MLCs), and piezoelectric devices.[1] $BaTiO_3$ undergoes a paraelectric to ferroelectric phase transition at the Curie temperature (T_C) of about 130 °C, associated with a sharp peak in the dielectric permittivity, and two other transitions below room temperature.[2] Specifically, Barium titanate doped with strontium (BST) is widely used in tunable RF capacitors for mobile phone applications due to its high dielectric response and tunability.[3,4] Improving BST's tunability would enhance the RF capacitor functionality. To do so, doping of BST was initially tempted, but the general observed trend is a decrease of the BST properties with dopants[5–7] while only a few dopants were found to improve the tunability of BST.[8–11] Another possibility is to look for other $BaTiO_3$-based systems to keep device integration close to the existing BST. Recently, the $(Ba,Ca)(Ti,Zr)O_3$ system has been attracting attention due to its high tunability, low dielectric losses, and reasonably large piezoelectric coefficient.[12–23] In particular, Liu and a coworker studied the system $(1-x)Ba(Ti_{0.8}Zr_{0.2})O_3$-$x(Ba_{0.7}Ca_{0.3})TiO_3$ which shows, for $x = 0.5$, a piezoelectric coefficient (d_{33}) of about 620 pm/V in ceramics[17] while it is reduced to about 70 and 80 pm/V for 350 nm and 600 nm thick films, respectively, with a tunability of 80% at about 330 kV cm^{-1},[19,22] due to the presence of a morphotropic phase boundary (MPB), similar to the $PbTiO_3$-$PbZrO_3$ (PZT) system. It is important at this point to notice that the addition of Zr in $BaTiO_3$ (BTZ) is known to reduce the paraelectric/ferroelectric transition temperature (T_c) as well as reducing the number of transitions from 3 to 1 (accompanied by a diffuse phase transition with a relaxor behavior) and displaying a maximum dielectric permittivity at room temperature for about 10%Zr.[24,25] A diffuse phase transition with a relaxor behavior is also observed with the addition of Ca in the BTZ system.[26] However, off-centering of Ca^{2+} ions on perovskite's A site has been shown to compensate for the reduction of ferroelectricity and lead to a stabilization or even more to an increase of the Curie temperature in BTO and BTZ, respectively.[27] Devices usually requiring materials in thin film form, and it is of interest to study the dependence of composition on thin film properties. It is our aim to explore part of the $BaTiO_3$-$BaTi_{0.7}Zr_{0.3}O_3$-$Ba_{0.7}Ca_{0.3}TiO_3$ phase diagram including the line studied by Liu and coworker. Ca doping is intended to minimize the effect of Zr doping on ferroelectricity while reducing the dielectric loss.[27] To do that, we produced samples with fixed Ca content and varied Zr doping. In this article, we would like to report on the 3%Ca library. A total of 600 capacitors were measured for this library in order to have a statistical analysis. Room temperature tunability and dielectric constant of the $Ba_{0.97}Ca_{0.03}Ti_{1-x}Zr_xO_3$ (BCTZ) thin films are non-monotonic across the gradient of composition, which is explained in terms of temperature dependence of the dielectric response versus composition but cannot be attributed to the presence of an MPB. Piezoelectric properties were also investigated and shown a decrease with increasing Zr content.

a)Electronic mail: christophe.daumont@univ-tours.fr
b)URL: http://www.greman.fr

II. EXPERIMENTAL SECTION

BCTZ thin films, with a thickness of about 130 nm, were deposited by combinatorial pulsed laser deposition (CPLD) technique[9] on IrO_2(≈140 nm)//Si(100) substrates (10 × 10 mm^2) using 3 targets: $BaTiO_3$, $BaTi_{0.7}Zr_{0.3}O_3$, and $Ba_{0.7}Ca_{0.3}TiO_3$. The laser fluence was set at 2 J cm^{-2}, the temperature at 700 °C and the oxygen pressure during deposition of 0.3 mbar. After deposition, 500 mbar of oxygen was introduced in the chamber. The sample was then cooled down to 400 °C at 3 °C min^{-1} and then kept for 1 hour at this temperature before cooling down to room temperature. DC sputtering (Plassys) was then used to deposit Au top electrodes via a shadow mask. A total of 600 capacitors (100 × 300 μm^2) are thus defined (12 per composition and around 50 compositions). However, 1.5 mm on each side of the sample was designed to have a constant composition, to distinguish between side effect and the effect of composition close to the edges of the sample, so that "only" about 35 different compositions between the 2 end members were measured. The capacitance measurements were performed using an Agilent 4294 a impedance analyzer and a cascade probe station. The measurements were performed at 100 kHz under an AC voltage of 50 mV and sweeping the DC voltage from 5 V to −5 V and then from −5 to 5 V. For the temperature measurements, some were performed with a Janis Probe station from 400 K to 80 K (first heating the sample, then measuring as it cools down at about 3 K/min) using a Keithley 590 CV analyzer, and some were performed after wire-bonding in a low temperature cell, from 80 K to 420 K, using a HP4192 impedance analyzer operating at 100 kHz with a AC voltage of 50 mV. The composition of the best device was measured by Rutherford back scattering (RBS), using 4He+ ion beams (2 MeV) with an incident angle of 5°, for a sample having a constant composition deposited on Si(100). The data were processed using SIMNRA software. Piezoelectric measurements were performed, at room temperature, using a double laser beam interferometer (DBLI, MSA-500 PolyTech). The measurement laser was focused on the top electrode where the probe was located, while the reference laser was focused on another top electrode to have a higher reflection than on the sample surface. The amplitude versus AC applied voltage was measured at 10 kHz. The piezoresponse-loop was measured under an AC voltage of 0.5 V, at 10 kHz, for an applied DC voltage ranging from −5.5 V to 5.5 V.

III. RESULTS AND DISCUSSION

A. Dielectric properties at room temperature

Figure 1 shows the upper part of the ternary phase diagram of the BTO-CTO-BZO system. The red line indicates the line of compositions investigated in this report, while the blue line shows the line for which some of compositions were studied by Ren and his coworker.[17] The inset shows the sample geometry for dielectric measurements: Part of the bottom electrode accessible (i.e., not covered by the dielectric) for the dielectric measurements. The gradient of color in the layer below Au shows the direction of the composition gradient. Figure 2(a) shows typical capacitance (C(V)) and

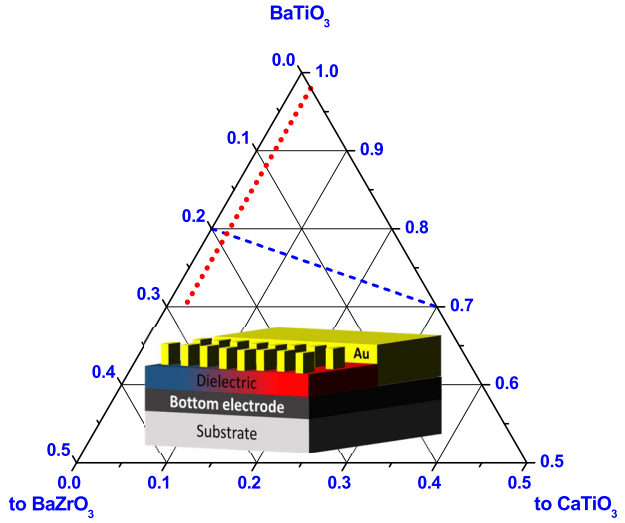

FIG. 1. Ternary phase diagram of the $BaTiO_3$-$BaZrO_3$-$CaTiO_3$. The red (dotted) line shows the line explored in the article while the blue (dashed) line corresponds to the line of composition studied in Ref. 17. The inset shows the geometry of the sample.

dielectric loss (Tan δ(V)) versus applied DC voltage for a randomly selected capacitor of the sample under interest here. The decrease of the dielectric loss as the voltage is increased reflects the typical behavior of a capacitor, which dielectric is a non-lossy ferroelectric. C(V) and Tan δ(V) curves are hysteretic and an offset is observed, probably due to the different nature of the electrodes. The values of both the maximum capacitance (C_{max}) and the corresponding voltage ($V_{C_{max}}$) for a given capacitor were extracted from the C(V) curves. The tunability at $V_{C_{max}} + 5V$ (to take into account the hysteretic behavior) is then defined as

$$tunability(\%) = \frac{C_{max} - C(V_{C_{max}} + 5V)}{C_{max}} * 100. \qquad (1)$$

Figures 2(b) and 2(c) show a 3D contour maps of the maximum capacitance of the capacitors and the tunability as a function of their location on the sample (and thus their composition), respectively. First, it is worth mentioning that on both graphs, an appreciable reproducibility of the results for all the lines of equal composition is observed (within ±3% for the capacitance and within ±3% for the tunability). From Figure 2(b), we can see that a maximum of C_{max} is located at intermediate compositions (%Zr ≈ 12.75% nominally). Interestingly, a local maximum is also seen at intermediate compositions for the tunability, but not at the same composition (%Zr ≈ 16.5% nominally, see Figure 2(c)). This implies that the maximum for the tunability is not directly related to the maximum in dielectric constant as the composition varies. It is to be noted that this first screening of the capacitance and tunability was performed up to 5 V and that the tunability could be even higher at higher field (up to the breakdown field).

For device performance, not only the tunability matters but also the dielectric loss (Tan δ). A way to take into account the dielectric losses of a tunable capacitor is in terms of the figure of merit (FoM), which is defined as

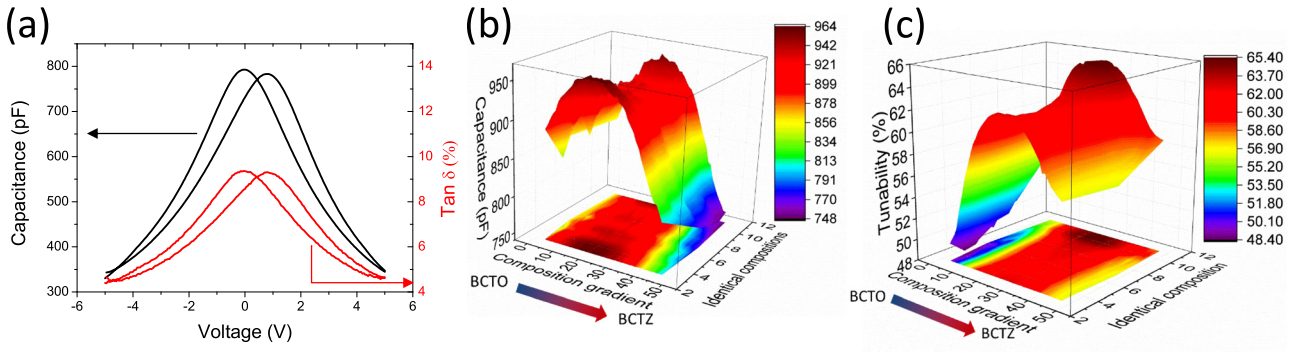

FIG. 2. (a) Typical capacitance (black line) and dielectric loss (red line) versus the applied voltage, in the case of a non-lossy ferroelectric capacitor. (b) 3D contour map of the maximum capacitance (C_{max}, pF) for all measured capacitors on one sample at room temperature (30 °C). (c) 3D contour map of the tunability (%) for the same sample.

$$\frac{Tunability(\%)}{\mathrm{Tan}\,\delta}. \quad (2)$$

Figure 3 shows the FoM (Tan δ taken at the same voltage as the tunability) as a function of the nominal Zr content (at room temperature) for all the measured devices. The addition of a few % of Zr improves drastically the FoM, as we find a value of 400 for 0%Zr and about 4 times more for the composition close to the maximum tunability (around 16.5%Zr). This cannot only be due to the increase of tunability (as it goes from around 50% to around 62%) as the Zr content increases, as we saw in Figure 2(c), but also to a decrease of the dielectric loss at a DC voltage of $V_{C_{max}} + 5V$ as the amount of Zr is increased, in agreement with previous report about the effect of Zr on the dielectric loss, tenability, and dielectric constant in Zr-doped $BaTiO_3$ ceramics.[28]

To clarify this issue, Figure 4 represents the normalized (to the 0 V value) dielectric losses as a function of the applied DC voltage for different compositions ranging from 0% to 9.75%. It is worth mentioning here that for every composition, the dielectric losses are within the range of 8% to 15% without an applied DC bias, but their evolution when a DC voltage is applied strongly differs. Indeed, in Figure 4, it can be seen that the dielectric losses first show a typical decrease at low bias (see Figure 2(a)) followed by an upturn (for example, 0%Zr at an applied voltage of about 4 V), reflecting the onset of leakage through the capacitor and the beginning of the breakdown. However, as the amount of Zr is increased (Figure 4), the upturn voltage increases and is even higher than 5 V for 9.75%Zr. Dielectric loss decrease upon Zr doping is usually attributed to the fact that Zr^{4+} is more chemically stable than Ti^{4+}, so that the hopping of electrons between Ti^{4+} and Ti^{3+} is reduced.[28,29] Moreover, this could reflect the decrease of Schottky emission due to an increase of the Schottky barrier height with the addition of Zr, consistent with what has been shown in BTZ (from 0.68 eV for 5%Zr doping to 1.24 eV for 25%Zr doping).[30]

Knowing that the work function of the electrodes used (IrO_2 and Au) is constant, implies a lowering of the electron affinity of BCTZ as the amount of Zr is increased, which is a very important result to improve the breakdown voltage of the devices and thus reach higher tunability values before the breakdown of the devices.

B. Temperature dependence of the dielectric response

To shed light on why the two maximums do not occur at the same composition as well as to determine the ferroelectric transition temperature (T_C), we performed capacitance measurements as a function of temperature (see Figure 5(a)).

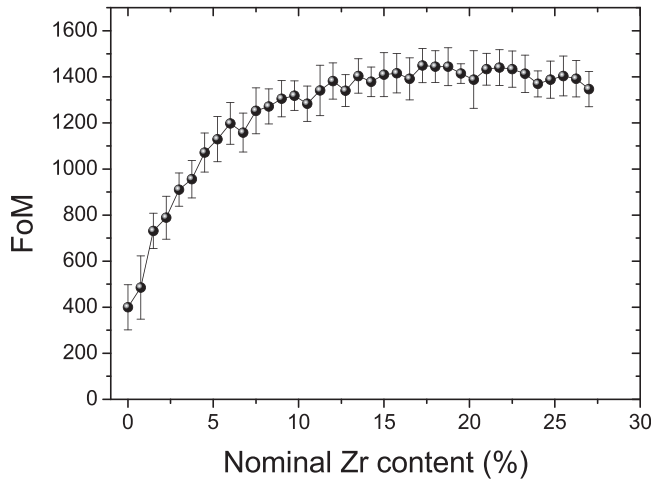

FIG. 3. Figure of Merit (FoM), at room temperature, as a function of the nominal Zr content for all the capacitors measured.

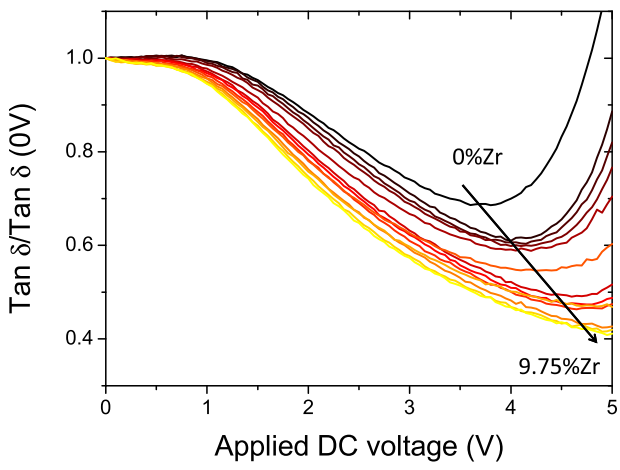

FIG. 4. Normalized dielectric loss as a function of applied DC voltage for different nominal Zr content ranging from 0% to 9.75%.

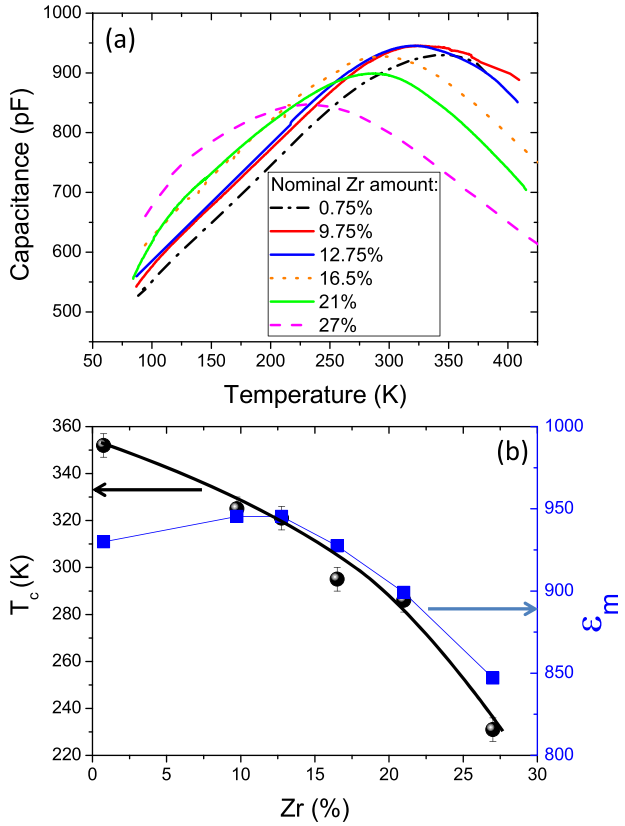

FIG. 5. (a) Real part of the dielectric permittivity as a function of temperature for a few selected compositions. (b) Temperature (dark dots) and value of the maximum of capacitance (C_m) (blue square) as a function of nominal Zr content. The lines are a guide to the eye.

In the figure, the different curves are indexed with respect to their nominal Zr content. It can be seen that, as the amount of Zr is increasing, the temperature (T_m) of the maximum capacitance (C_m to distinguish from C_{max} of the C(V) curves) decreases. This is due to the lowering of the ferroelectric transition temperature as the amount of Zr increases, as in the ceramics of $BaTi_{1-x}Zr_xO_3$.[31] From this figure, we can also explain the maximum value of the capacitance of Figure 2(b): As the amount of Zr increases, the overall capacitance increases slightly to reach a maximum and then decreases as more Zr is added (Figure 5(b)), as observed in BTZ thin films prepared by RF sputtering.[28]

Simultaneously, T_C is decreasing (Figure 5(b)) and the maximum tunability is reached at the composition which has its T_c at room temperature,[32] explaining why the maximum of the capacitance and tunability do not occur at the same compositions. It is also now clear that the room temperature maximum of tunability of Figure 2(c) is solely due to the ferroelectric transition, since the highest tunability is observed for the composition that has its T_C at room temperature.

The extraction of T_m and C_m (and thus ϵ_m) from this measurement allows us to determine the diffuseness of the phase transition, for a given composition, using a modified Curie–Weiss law[33]

$$\frac{1}{\epsilon} - \frac{1}{\epsilon_m} = \frac{(T - T_m)^\gamma}{C}, \tag{3}$$

where γ and C are constants and the value of γ, giving some information about the character of the phase transition, ranges from 1 (ferroelectric phase transition) to 2 (complete diffuse phase transition). Thus, plotting $\mathrm{Ln}\left(\frac{1}{\epsilon} - \frac{1}{\epsilon_m}\right)$ versus $\mathrm{Ln}((T - T_m)$ should give straight line, whose slope corresponds to γ. This is shown in Figure 6 for the different compositions measured in 5 (a) (the color code being the same).

We indeed obtain straight lines which allows us to determine the value of γ to be 1.867 (±0.005), 1.887 (±0.003), 1.783 (±0.003), 1.719 (±0.006), 1.76 (±0.043), and 1.794 (±0.167) for 27%, 21%, 16.5%, 12.75%, 9.75%, and 0.75%Zr, respectively. The increasing errors are due to the reduction of the number of data points above T_c and, thus, the poor fit to the data (since the data need to be fitted far above T_c). However, we can see a general increase of γ as the amount of Zr is increased which is due to increasing composition disorder as more Zr is introduced. The overall high value for γ (close to 1.7 for almost pure $BaTiO_3$) is not surprising and is usually due to the microstructure nature of the thin films compared to their ceramics counterpart (e.g., finer grain size and residual strain) as observed in many systems when put under thin film form.[34–37] In any case, the system behaves similarly to the ceramics,

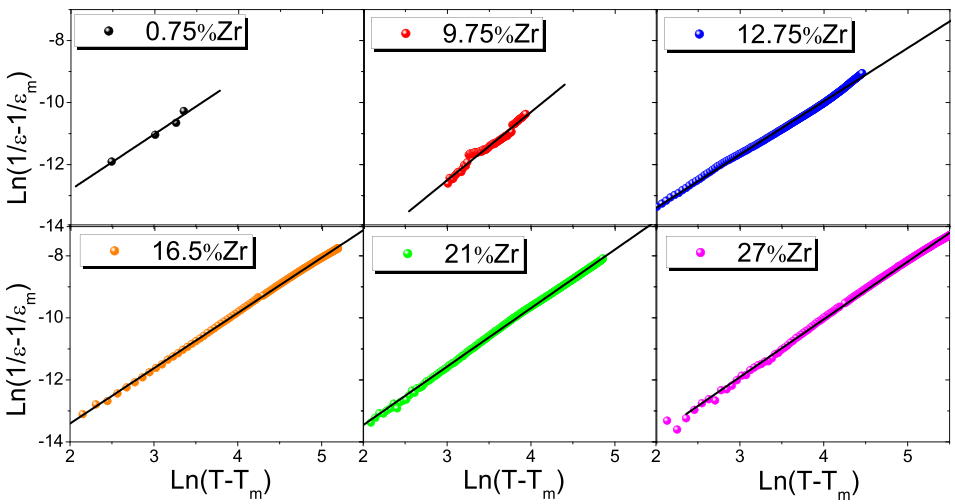

FIG. 6. $\mathrm{Ln}(1/\epsilon\text{-}1/\epsilon_m)$ as a function of $\mathrm{Ln}(T\text{-}T_m)$ extracted from Figure 5(a) for different concentrations of Zr. The black lines are the linear fits to the data.

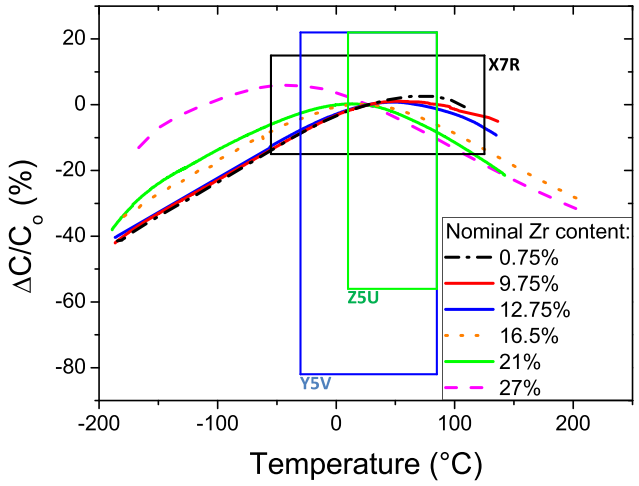

FIG. 7. TCC of the BCTZ library as a function of temperature for different compositions spanning the whole range of compositions.

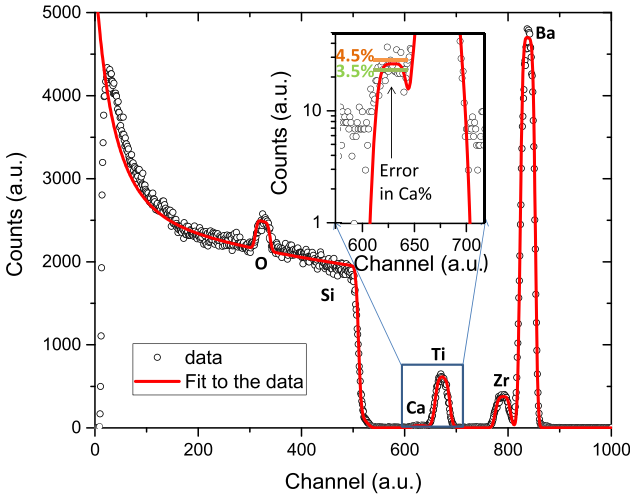

FIG. 8. RBS spectra for a film having the nominal composition close to the capacitors showing the maximum of tunability. The inset shows a zoom on the plateau corresponding to Ca, used to evaluate the error on the Ca content.

that is to say that the increase of the amount of Zr leads to a more diffuse transition, which can be indicative of a possible relaxor effect.[25] The temperature dependence of the dielectric response at different frequencies would shine light on this issue but are out of the scope of this study.

For practical application of the capacitors, another aspect concerns the thermal stability of their dielectric responses over a considered temperature range. Even though the capacitance varies too much for class I capacitors, one can wonder about the temperature capacitance coefficient (TCC) for this simple metal–insulator–metal (MIM) capacitors, compared to multi-layers ceramics capacitors (MLCC).[38]

The TCC of our library, defined as $\frac{C(T)-C_0}{C_0} * 100\,(\%)$, where C_0 is the room temperature capacitance and C(T) is the capacitance at a given temperature, is shown in Figure 7 as a function of temperature for different compositions corresponding to the ones in Figure 5. The different boxes in the figure correspond to the different requirements of the class II capacitors. From this figure, all the compositions are within the Y5V requirements ($-82\% \leq \Delta C/C \leq +22\%$ from $-30\,^{\circ}C$ to $85\,^{\circ}C$), but most importantly, a wide range of compositions meet the X7R requirements ($-15\% \leq \Delta C/C \leq +15\%$ from $-55\,^{\circ}C$ to $125\,^{\circ}C$). Some could also possibly meet the requirements for X8R ($-15\% \leq \Delta C/C \leq +15\%$ from $-55\,^{\circ}C$ to $150\,^{\circ}C$), but the compositions that could meet those requirements were not measured up to $150\,^{\circ}C$, so it is difficult to be sure that they would meet the requirements. Finally, the composition at (and around) maximum tunability also meets the requirements for X7R type of class II capacitors on top of being promising for tunable devices.

C. Composition at maximum tunability

So far, we have been using the nominal Zr content in this study but it is important to verify the compositions, at least for the capacitor presenting the best tunability at room temperature. It is important to note that Energy-Dispersive X-ray Spectroscopy (EDS or EDX) was attempted, but the very strong overlap between the Ba and Ti peaks made the exact ratio of Ba and Ti impossible to determine (principle lines: $Ba_{L\alpha} = 4.4663\,keV$ and $Ti_{K\alpha} = 4.5089\,keV$).

To do so, a reproduction of the sample with constant composition aimed to be composition presenting maximum tunability was deposited on Si(100) ($10 \times 10\,mm^2$), and RBS measurements were performed. The data and the fit to the data to extract the composition are shown in Figure 8. The inset shows a zoom around the plateau used to calculate the Ca content. It can be seen that the overall fit is good, so the extracted composition can be considered accurate even though the Ca plateau is not perfectly defined; it was still possible to attribute a range for the Ca content in the films.

Table I summarizes the amount of different elements, the ratio of A site to B site of the perovskite, as well as the ratios of cations on A and B sites. The measured ratios of the cations on A-site (0.04) and B-site (0.167) are close to the expected nominal ratios of 0.03 and 0.165, respectively, of the corresponding capacitor in the composition spread sample. We can thus safely assume that the nominal compositions are close to the real compositions even though a slight excess of 6% of site A with respect to site B seems present and that a slight excess of 1%Ca is present in the films. However, the signal-to-noise ratio is about 3/1 with a background signal representing 30% of the Ca signal so taking that into account would bring the ratio closer to the expected value of 0.03. Now that we understand the origin of the local maximum of the dielectric constant and tunability, and we can now investigate the piezoelectric response of the library.

TABLE I. Composition from RBS measurements.

%at.Ba	%at.Ca	%at.Ti	%at.Zr	%at.O
18.00	0.80	15.00	2.80	63.40
$\frac{Ba+Ca}{Ti+Zr}$		$\frac{Ca}{Ca+Ba}$	$\frac{Zr}{Ti+Zr}$	
1.06		0.04	0.167	

D. Piezoelectric properties of the library

To investigate the room temperature piezoelectric properties of the library, a double laser interferometer (DBLI) was used. This allows the precise measurement of the piezoelectric properties while being able to subtract the contribution from the substrate bending.[39] The first experiment on a capacitor was to measure the standard deviation of the measurements. To do so, each capacitor was measured, in fixed conditions, 10 times, and the standard deviation was calculated for each capacitor and then averaged to have an overall standard deviation of less than 1 pm (not shown here).

We then measure the effective piezoelectric coefficient (d_{33}^{eff}), defined, in the case of thin films, as:

$$d_{33}^{eff} = d_{33} - \frac{2s_{13}^{E}}{s_{11}^{E} - 2s_{12}^{E}} d_{31} \tag{4}$$

with d_{33} and d_{31} being the piezoelectric constants and s_{1n}^{E} (with $n = 1$ to 3) being the bulk elastic stiffness at constant electric field (E). The reduction of the piezoelectric coefficient with respect to the bulk ($d_{33}^{eff} < d_{33}$ from Equation (4)) is due to the clamping of the material on a substrate.[40]

Under an applied voltage $V = V_0\cos(\omega t)$, the sample surface would then vibrate with the form $\Delta z = \Delta Z_0\cos(\omega t + \Phi)$ ($\Phi = 0°$ if the polarization is parallel to the applied field and $\Phi = 180°$ if antiparallel) with $\Delta Z_0 = d_{33}^{eff} V_0$.[41] Using the DBLI, the sample vibration (displacement) is measured via the Doppler effect, and from the previous equation, the slope of the displacement versus the AC applied voltage amplitude gives d_{33}^{eff}. Such a plot is shown in Figure 9 for the different compositions presented in the temperature dependence section.

It can be seen that the data depart from the linear behavior at about 3 V. While a superlinear behavior is usually attributed to the contribution of the ferroelastic domain wall motion,[42,43] sublinear behavior has been attributed to depoling effects under high enough AC field[44] as observed in our data. Thus, linear fits from 0 to 3 V were used to measure d_{33}^{eff}. Also, as the amount of Zr is increased, the slope is decreasing, implying a decreasing d_{33}^{eff}. Figure 10 shows the extracted d_{33}^{eff} values as a function of the Zr content for the whole range of measured compositions, for 3 measured lines (so 3 measurements per compositions and about 35 compositions).

The values of d_{33}^{eff} are monotonically decreasing as the amount of Zr is increased from about 30 pm/V below 5%Zr down to around 15 pm/V for 25%Zr. Knowing that the d_{33}^{eff} is maximum close to T_C, this evolution does not reflect the decrease of T_C with the composition.[40] Moreover, even though we were able to have a composition induced increase of the dielectric constant at room temperature, this increase cannot be attributed to the presence of an MPB in this system, since both the polarization and the piezoelectric coefficient should also show an increase if it was the case. Instead, the room temperature properties are dictated by two effects: (i) an increase of the dielectric constant for small amounts of Zr and (ii) the decrease of T_C with the continuous addition of Zr. Since the polarization is proportional to the piezoelectric coefficient, measuring a so-called "d_{33} loop" should reflect the ferroelectric behavior under applied DC voltage.

Figure 11 shows d_{33} loops for the different compositions ranging from 0.75%Zr to 27%Zr. It can be seen that the loops are reasonably well saturated and the value of the "saturated" d_{33}^{eff} decreases with the increasing amount of Zr, as expected from the displacement versus applied AC voltage. Interestingly, the coercive field is very small (so small that it cannot be accurately extracted from the data because of the lack of data points near it) and seems to increase with increasing Zr content. Moreover, as the bias is increased, the d_{33}^{eff} increases very sharply and then saturates. This behavior is not expected for a ferroelectric material, but a recent work showed that the field at which the maximum piezoelectric coefficient is reached could be smaller than the polarization coercive field in polycrystalline ceramics of $93\%(Bi_{1/2}Na_{1/2})TiO_3$–$7\%BaTiO_3$ and is attributed to the coalescence of polar nano-regions.[45] We suggest that similar effect is occurring at specially low level of dopings and emphasized in thin film form compared to the polycrystalline ceramics due to reduced dimensions and would dominate the

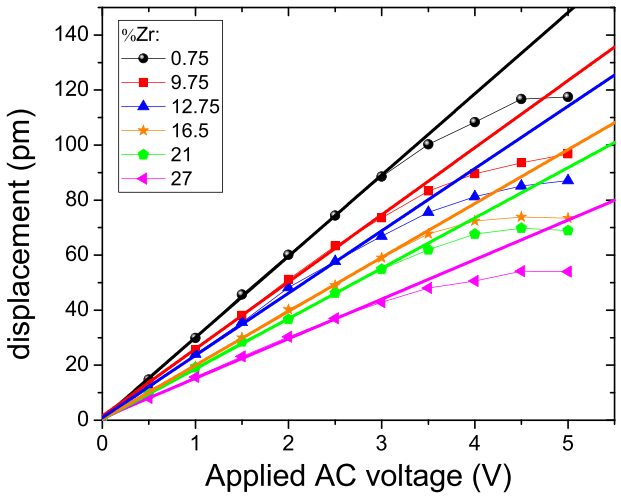

FIG. 9. Displacement as a function of applied AC voltage for different Zr amount corresponding to previous figures. The color code is the same. The thick straight lines are linear fits, from 0 to 3 V of the data.

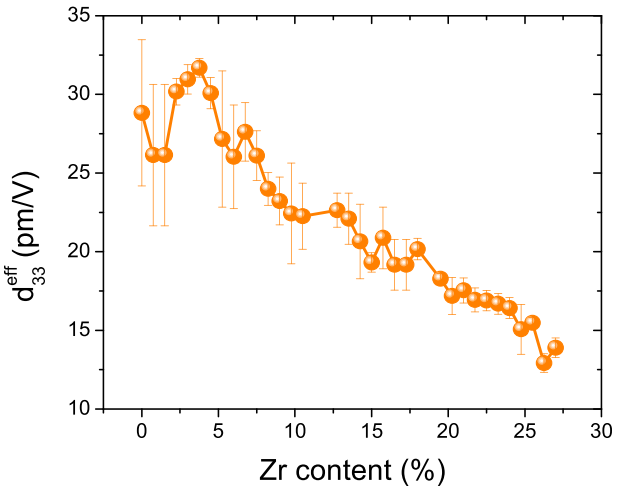

FIG. 10. d_{33}^{eff} as a function of Zr content.

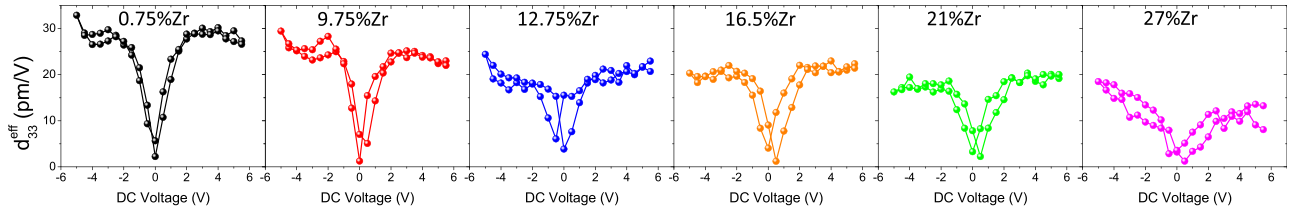

FIG. 11. d_{33}^{eff} as a function of applied DC voltage for different amount of Zr. From left to right: 0.75%*Zr*, 9.75%*Zr*, 12.75%*Zr*, 16.5%*Zr*, 21%*Zr*, and 27%*Zr*.

response. Moreover, piezoelectric activity is still present even above T_C, which can be another indication of the presence of nano-polar regions which persist above T_C in the non-polar matrix, similarly to what has been observed in $0.5Ba(Ti_{0.8}Zr0.2)O_3–0.5(Ba_{0.7}Ca_{0.3})TiO_3$ ceramics.[46] Further work, including measurements of the polarization and frequency dependence of the capacitance versus temperature, should clarify this aspect but is out of scope of this paper.

IV. CONCLUSION

We successfully deposited BCTZ polycrystalline thin films library on IrO_2//Si(100) substrates using CPLD. We show that CPLD is a powerful technique to study continuous lines of the $BaTiO_3$-$BaTi_{0.7}Zr_{0.3}O_3$-$Ba_{0.7}Ca_{0.3}TiO_3$ phase diagram (or any other phase diagram) in thin film form, which is crucial for their integration into devices, and allows comparison with their bulk counterpart to an extended level as they are likely to differ. Particularly, we were able to determine a composition with maximum tunability and to understand the origin of this maximum in relation to the shift of T_C with Zr content, leading to having T_C equating room temperature for this composition. We also demonstrated the use of the addition of Zr to reduce the breakdown voltage of the devices by an increase of the Schottky barrier height. We also shown that many of the studied compositions meet the requirements for class II X7R capacitors for a MIM capacitor, which could be of interest for the miniaturization of the device at low operating powers. Finally, we show that the piezoelectric coefficient follows the expected behavior of the polarization, that is to say a decrease with the increase of Zr content, due to the lowering of the T_C towards the low temperature.

ACKNOWLEDGMENTS

This work was supported by the French government and STMicroelectronics through part of the project Investissements d'Avenir Tours2015 as well as by the Région Centre through the project OXYMORE. The authors would like to thank Cécile Autret Lambert and Sylvain Roger for the PLD targets preparation. We also would like to thank Guillaume Géguan for useful discussions.

[1]F. D. Morrison, D. C. Sinclair, and A. R. West, Int. J. Inorg. Mater. **3**, 1205 (2001).
[2]T. Lee and I. A. Aksay, Cryst. Growth Des. **1**, 401 (2001).
[3]P. Bao, T. J. Jackson, and M. J. Lancaster, J. Phys. D **41**, 063001 (2008).
[4]G. Subramanyam, M. W. Cole, N. X. Sun, T. S. Kalkur, N. M. Sbrockey, G. S. Tompa, X. Guo, C. Chen, S. P. Alpay, G. A. Rossetti, Jr., K. Dayal, L.-Q. Chen, and D. G. Schlom, J. Appl. Phys. **114**, 191301 (2013).
[5]M. W. Cole, P. C. Joshi, and M. H. Ervin, J. Appl. Phys. **89**, 6336 (2001).
[6]M. W. Cole, P. C. Joshi, M. H. Ervin, M. C. Wood, and R. L. Pfeffer, Thin Solid Films **374**, 34 (2000).
[7]J. S. Horwitz, W. Chang, A. C. Carter, J. M. Pond, S. W. Kirchoefer, D. B. Chrisey, J. Levy, and C. Hubert, Integr. Ferroelectr. **22**, 279 (1998).
[8]R.-V. Wang, P. C. McIntyre, J. D. Baniecki, K. Nomura, T. Shioga, K. Kurihara, and M. Ishii, Appl. Phys. Lett. **87**, 192906 (2005).
[9]G. Liu, J. Wolfman, C. Autret-Lambert, J. Sakai, S. Roger, M. Gervais, and F. Gervais, J. Appl. Phys. **108**, 114108 (2010).
[10]M. W. Cole, C. Hubbard, E. Ngo, M. Ervin, M. Wood, and R. G. Geyer, J. Appl. Phys. **92**, 475 (2002).
[11]Y.-A. Jeon, T.-S. Seo, and S.-G. Yoon, Jpn. J. Appl. Phys., Part 1 **40**, 6496 (2001).
[12]T. S. Kalkur and W. C. Yi, Integr. Ferroelectr. **45**, 123 (2002).
[13]T. S. Kalkur, W. C. Yi, E. Philofsky, and L. Kammerdiner, Mater. Lett. **57**, 4147 (2003).
[14]X. G. Tang, K. H. Chew, J. Wang, and H. L. W. Chan, Appl. Phys. Lett. **85**, 991 (2004).
[15]N. Cramer, E. Philofsky, L. Kammerdiner, and T. S. Kalkur, Appl. Phys. Lett. **84**, 771 (2004).
[16]X. G. Tang and H. L. W. Chan, J. Appl. Phys. **97**, 034109 (2005).
[17]W. Liu and X. Ren, Phys. Rev. Lett. **103**, 257602 (2009).
[18]L. L. Jiang, X. G. Tang, Q. Li, and H. L. W. Chan, Vacuum **83**, 1018 (2009).
[19]A. Piorra, A. Petraru, H. Kohlstedt, M. Wuttig, and E. Quandt, J. Appl. Phys. **109**, 104101 (2011).
[20]F. Benabdallah, A. Simon, H. Khemakhen, C. Elissalde, and M. Maglione, J. Appl. Phys. **109**, 124116 (2011).
[21]V. S. Puli, A. Kumar, D. B. Chrisley, M. Tomozawa, J. F. Scott, and R. S. Katiyar, J. Phys. D: Appl. Phys. **44**, 395403 (2011).
[22]G. Kang, K. Yao, and J. Wang, J. Am. Ceram. Soc. **95**, 986 (2012).
[23]V. S. Puli, D. K. Pradhan, S. Adireddy, R. Martinez, P. Silwal, J. F. Scott, C. V. Ramana, D. B. Chrisey, and R. S. Katiyar, J. Phys. D: Appl. Phys. **48**, 355502 (2015).
[24]M. Aghayan, A. K. Zak, M. Behdani, and A. M. Hashim, Ceram. Int. **40**, 16141 (2014).
[25]J. Ravez, C. Broustera, and A. Simon, J. Mater. Chem. **9**, 1609 (1999).
[26]S. D. Chavan and D. J. Salunkhe, Int. J. Sci. Res. **3**, 1557 (2014); available at http://www.ijsr.net/archive/v3i11/T0NUMTQxMjc5.pdf.
[27]D. Fu and M. Itoh, *Ferroelectric Materials—Synthesis and Characterization*, edited by A. Peláiz-Barranco (InTech, 2015).
[28]T. B. Wu, C. M. Wu, and M. L. Chen, Appl. Phys. Lett. **69**, 2659 (1996).
[29]W. S. Choi, B. S. Jang, D.-G. Lim, J. Yi, and B. Hong, J. Cryst. Growth **237–239**, 438 (2002).
[30]F. M. Pontes, M. T. Escote, C. C. Escudeiro, E. R. Leite, E. Longo, A. J. Chiquito, P. S. Pizani, and J. A. Varela, J. Appl. Phys. **96**, 4386 (2004).
[31]L. Dong, D. S. Stone, and R. S. Lakes, J. Appl. Phys. **111**, 084107 (2012).
[32]A. K. Tagantsev, V. O. Sherman, K. F. Astafiev, J. Venkatesh, and N. Setter, J Electroceram. **11**, 5 (2003).
[33]S. Mahajan, O. P. Thakur, D. K. Bhattacharya, and K. Sreenivas, J. Appl. Phys. **42**, 065413 (2009).
[34]R. P. S. M. Lobo, N. D. S. Mohallen, and R. L. Moreira, J. Am. Ceram. Soc. **78**, 1343 (1995).
[35]S. Tong, M. Narayanan, B. Ma, R. E. Koritala, S. Liu, U. B. Balachandran, and D. Shi, Acta Mater. **59**, 1309 (2011).
[36]C. M. Carlson, T. V. Rivkin, P. A. Parilla, J. D. Perkins, D. S. Ginley, A. B. Kozyrev, V. N. Oshadchy, and A. S. Pavlov, Appl. Phys. Lett. **76**, 1920 (2000).

[37]M. Jain, S. B. Majumder, R. S. Katiyar, F. A. Miranda, and F. W. van Keuls, Appl. Phys. Lett. **82**, 1911 (2003).
[38]S.-H. Wang, W.-H. Lee, Y.-L. Tsai, and Y.-C. Lee, Int. J. Appl. Ceram. Technol. **12**, E25 (2015).
[39]A. L. Kholkin, C. Wutchrich, D. V. Taylor, and N. Setter, Rev. Sci. Instrum. **67**, 1935 (1996).
[40]A. L. Kholkin, N. A. Pertsev, and A. V. Goltsev, *Piezoelectric and Acoustic Materials for Transducer Applications*, edited by A. Safari and E. K. Akdoğan (Springer, 2008).
[41]A. Gruverman and S. V. Kalinin, J. Mater. Sci. **41**, 107 (2006).
[42]S. Trolier-McKinstry, N. B. Gharb, and D. Damjanovic, Appl. Phys. Lett. **88**, 202901 (2006).
[43]N. B. Gharb, S. Trolier-McKinstry, and D. Damjanovic, J. Appl. Phys. **100**, 044107 (2006).
[44]V. V. Shvartsman, N. A. Perstev, J. M. Herrero, C. Zaldo, and A. L. Kholkin, J. Appl. Phys. **97**, 104105 (2005).
[45]H. Guo, C. Ma, X. Liu, and X. Tan, Appl. Phys. Lett. **102**, 092902 (2013).
[46]D. Damjanovic, A. Biancoli, L. Batooli, A. Amirhossein, and J. Trodahl, Appl. Phys. Lett. **100**, 192907 (2012).